Serpentinite-Hosted Nickel-, Iron-, and Cobalt- Sulfide, Arsenide, and Intermetallic Minerals in an Unusual Inland Tectonic Setting, Southwest Arizona

James H. Wittke[1], Gordon B. Haxel[2,1], Gabe S. Epstein[2], and Carl E. Jacobson[3,4]

[1]Northern Arizona University; [2]USGS, Flagstaff; [3]Iowa State University; [4]West Chester University of Pennsylvania

Peridotite and unusual minerals in southwest Arizona

Southern Arizona is an inboard realm of intermediate to silicic Paleoproterozoic continental crust heavily overprinted by Mesoproterozoic, Mesozoic, and Cenozoic continental magmatism, largely silicic. Within this continental region, we recently discovered blocks of oceanic mantle peridotite, in the early Paleogene Orocopia Schist low-angle subduction complex (Jacobson et al., 2011) exposed at Cemetery Ridge, southwest Arizona (Fig. 1; Haxel et al., 2015). This peridotite (Fig. 2) is of two types—harzburgite (including olivine orthopyroxenite) and serpentinite derived from dunite. The peridotite was serpentinized by seawater. Oceanic peridotite is strikingly out-of-place in southwest Arizona. Correspondingly, we have found several serpentinite-hosted sulfide, arsenide, and intermetallic minerals that are new to, or rare in, Arizona. One of these minerals, orcélite, is also rare globally.

Whole-rock geochemistry

In the Cemetery Ridge (CR) peridotite, sulfur declines by a factor $\gtrsim 15$ with increasing serpentinization (Fig. 3A); but concentrations of chalcophile trace elements differ little between partially serpentinized harzburgite and serpentinite (Fig. 3B). Median concentrations of 14 chalcophile elements range from ~ 1000 µg/g for Ni to ~ 10 ng/g for Pt and Pd. Minerals found so far qualitatively account for seven of the eight elements with concentration > 0.3 µg/g. For example, Bi, 0.6 µg/g, is represented by rare bismuthinite.

Opaque minerals

The most common opaque mineral in CR serpentinite is relatively abundant (≈ 3–5 %) magnetite, intimately intergrown with mesh-textured serpentine (Fig. 2B) derived from olivine. Examination by SEM and EMP reveals that magnetite encloses and is intergrown with far less abundant, but ubiquitous, small (~ 30–100 µm) grains of pentlandite, cobaltoan pentlandite, and heazlewoodite. One rock also contains troilite. Six additional minerals are even less abundant, typically several tiny (~ 3–20 µm) grains per thin section: bornite, maucherite, orcélite, awaruite, bismuthinite, and parkerite(?). Despite the difficulty of analyzing small grains by EMP, compositions of these minerals closely match those from other localities (e.g., Table 1).

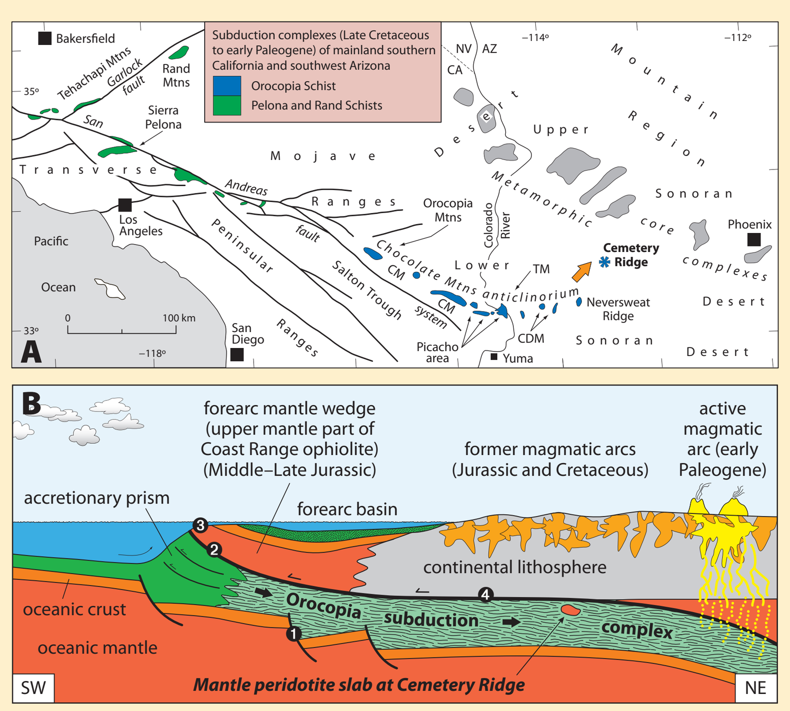

Figure 1. (A) Exposures of the low-angle subduction complex underlying most of southern California and much of Arizona, showing location of the recently discovered body of peridotite-bearing Orocopia Schist at Cemetery Ridge, southwest Arizona. Orange arrow indicates direction of subduction, based on the orientation of prograde lineation (Jacobson et al., 1988; Haxel et al., 2002) and seismic anisotropy data (Porter et al., 2011). **(B)** Low-angle subduction system beneath southern California and southwest Arizona, showing four tectonic settings where the subducted mantle peridotite at CR could have originated (Haxel et al., 2015). Geochemical evidence favors possibility ❷ or ❸.

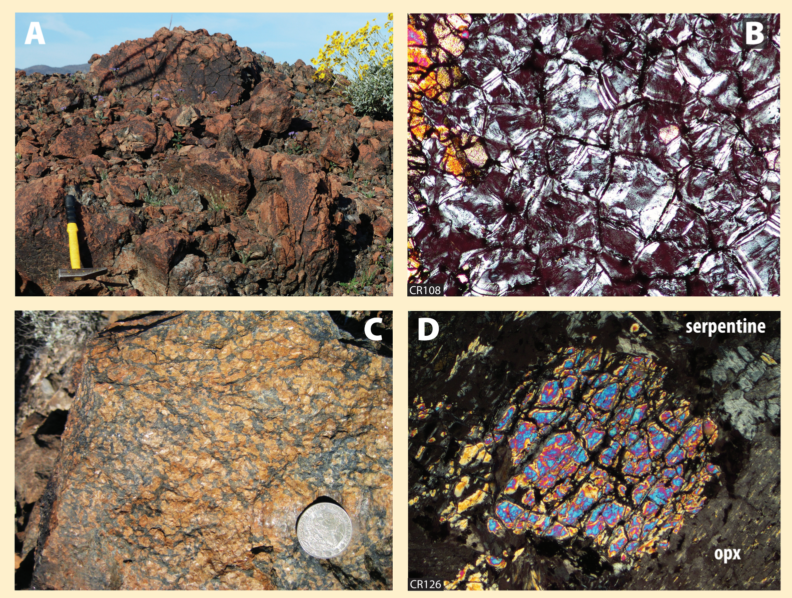

Figure 2. Peridotite, Cemetery Ridge, southwest Arizona. **(A)** Serpentinite. **(B)** Serpentinite: mesh-textured serpentine after olivine, magnetite, minor relict olivine (upper left). XP; FOV 1 mm. **(C)** Coarse-grained harzburgite: orthopyroxene (red-brown), serpentinized olivine (black). Coin, 33 mm. **(D)** Slightly serpentinized olivine in harzburgite. XP; 1.6 mm.

Pentlandite and cobaltoan pentlandite

Pentlandite (Fig. 4), a characteristic mineral of serpentinites (Frost, 1985; Klein and Bach, 2009), is the dominant sulfide at CR (Figs. 6–8). Pentlandite [$(Fe,Ni)_9S_8$, Fe ~ Ni] and Co pentlandite [Co_9S_8] are considered distinct minerals (Gaines et al., 1997). These two compositions are immiscible at low temperature, but form a solid-solution series, through cobaltoan pentlandite, at higher temperatures (Fig. 5). CR pentlandite compositions support the contention of Haxel et al. (2015) that serpentinization took place at fairly high temperature.

CR pentlandite has an unusually wide range of molar Ni/Fe, 0.8 to 6, and Co/(Fe+Ni+Co) as great as 74 %. The compositional gap between pentlandite and cobaltoan pentlandite at CR is similar to that found by Klein and Bach (2009) for pentlandite from the Mid-Atlantic Ridge.

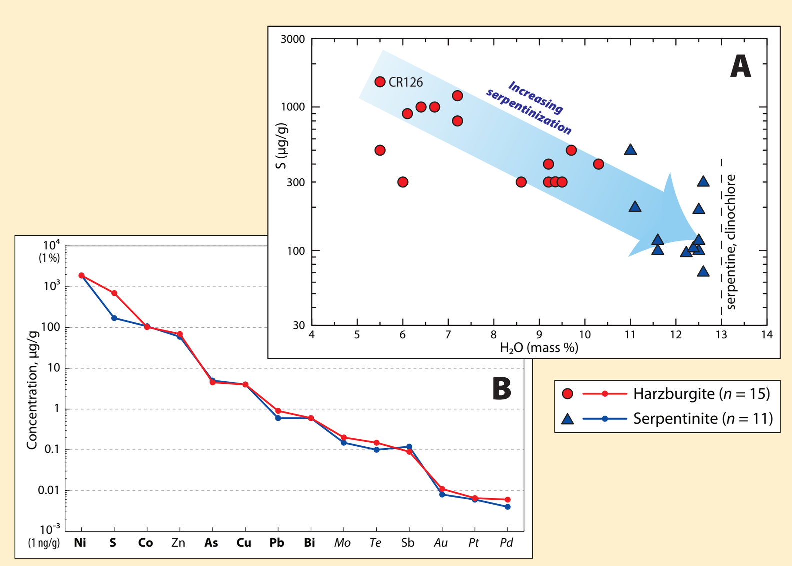

Figure 3. (A) Decline of whole-rock S with increasing H_2O and degree of serpentinization. **(B)** Median whole-rock concentration (µg/g) of 14 chalcophile trace elements. **Bold**, elements qualitatively accounted for by minerals found in CR peridotite (see text); *italic*, elements not analyzed (by choice) by EMPA.

Heazlewoodite, Ni_3S_2

Heazlewoodite, the most S-poor of the five Ni-sulfide minerals (Fig. 4), is another characteristic phase of serpentinites, and also occurs in a few other types of ultramafic rocks and in meteorites (e.g. Allende). Other than CR, heazlewoodite is known from nine localities in the western United States, six of which are in serpentinites of the California and Oregon Coast Ranges. CR heazlewoodite (Figs. 7–9) is near-ideal, with only minor Fe replacing Ni; and similar to heazlewoodite from, for example, the Mid-Atlantic Ridge (Table 1).

Troilite; bornite

Troilite occurs in only one rock, the least-serpentinized harzburgite, with the highest concentration of sulfur (CR126; Fig. 3A). Troilite partially replaces pentlandite (Fig. 6). Its composition is $Fe_{7.87}S_8$, much closer to troilite (FeS) than to typical pyrrhotite ($Fe_{7.00-7.33}S_8$; Bowles et al., 2011), the more common mineral in serpentinite.

We've found bornite, $Cu_{4.96}Fe_{1.17}S_4$, intergrown with pentlandite, within one magnetite grain in one serpentinite (Fig. 7D).

Nickel arsenides: orcélite, $Ni_{4.75}As_2$; and maucherite, $Ni_{11}As_8$

Six Ni-arsenide minerals are known, with As/Ni from 0.42 to 2.0 (Table 2). At CR we've found the two low-As members of this group: orcélite and maucherite (Table 1). Orcélite is in general nonstoichiometric: $(Ni+Fe)_xAs_2$, $4.18 \le x \le 5.49$; ideally $x = 4.75$ (Lorand and Pinet, 1984; Bindi et al., 2014). CR orcélite averages $x = 4.47$.

These two arsenide minerals typically lie along the margin of magnetite, just inside or just outside (Figs. 7C, 9D). This arrangement suggests reaction with, or inward migration of As from, the surrounding serpentine matrix, consistent with evidence that As (as As^{5+}, possibly substituting for Si[4]) can reside in serpentine (Hattori et al., 2005).

In the western U.S., orcélite has previously been reported from only one locality, in southwest Oregon; and maucherite from one place in the northwest corner of California (www.mindat.org).

Table 1. Structural formulae, ideal and average, of sulfide and arsenide minerals.

Mineral	Ideal	Cemetery Ridge	Other locality	Area	Ref.
pentlandite	$(Fe,Ni)_9S_8$	$(Fe_{3.97}Ni_{4.67}Co_{0.24})_{8.89}S_8$	$(Fe_{4.08}Ni_{4.65}Co_{0.18})_{8.90}S_8$	15°20´ N FZ, Mid-Atlantic Ridge	Klein and Bach, 2009
cobaltoan pentlandite	$(Fe,Ni,Co)_9S_8$	$(Fe_{1.22}Ni_{3.32}Co_{4.55})_{9.08}S_8$	$(Fe_{1.61}Ni_{2.62}Co_{5.08})_{9.31}S_8$	15°20´ FZ, Mid-Atlantic Ridge	Klein and Bach, 2009
heazle-woodite	Ni_3S_2	$(Ni_{2.89}Fe_{0.10})_{2.99}S_2$	$(Ni_{2.91}Fe_{0.13})_{3.04}S_2$	15°20´ FZ, Mid-Atlantic Ridge	Klein and Bach, 2009
orcélite	$Ni_{4.75}S_2$	$(Ni_{4.38}Fe_{0.08})_{4.47}As_2$	$(Ni_{4.86}Fe_{0.05})_{4.92}As_2$	Baberton, South Africa	Bindi et al., 2014
maucherite	$Ni_{11}As_8$	$(Ni_{10.26}Fe_{0.74})_{11.00}(As_{7.93}S_{0.07})_8$	$(Ni_{11.06}Fe_{0.27})_{11.33}(As_{7.89}S_{0.11})_8$	Beni Bousera, Morocco	Lorand and Pinet, 1984

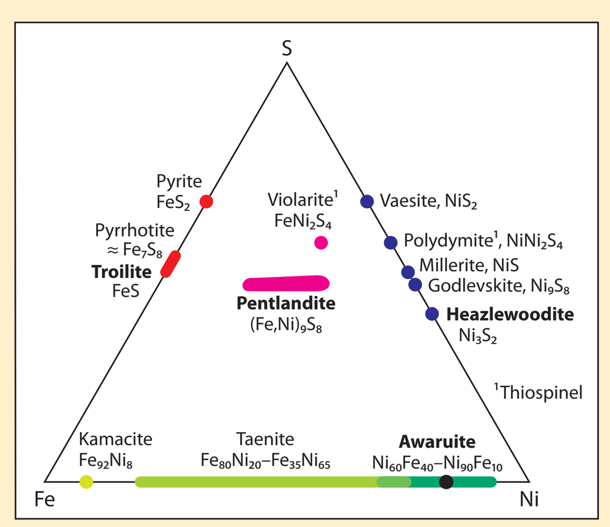

Figure 4. Ideal composition (molar proportions) of some principal minerals of the Fe-Ni-S system (after Harris and Nickel, 1972). **Bold** type indicates minerals found in CR serpentinite. Compositional range of awaruite from Sciortino et al. (2015); CR awaruite indicated by black dot.

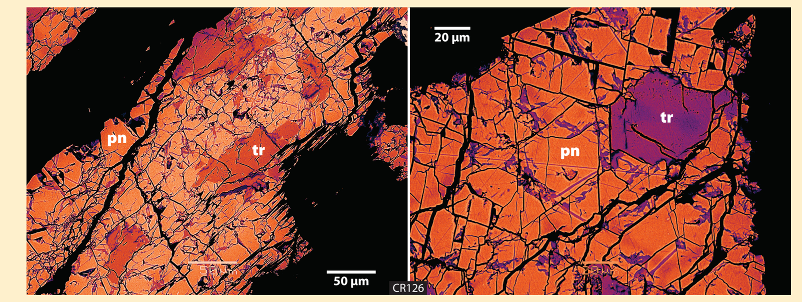

Figure 6. Patchy and blocky replacement of pentlandite (pn) by troilite (tr). Back-scattered-electron images, false-color. In all BSE images (Figs. 6–9), black-colored matrix or background is largely or entirely serpentine.

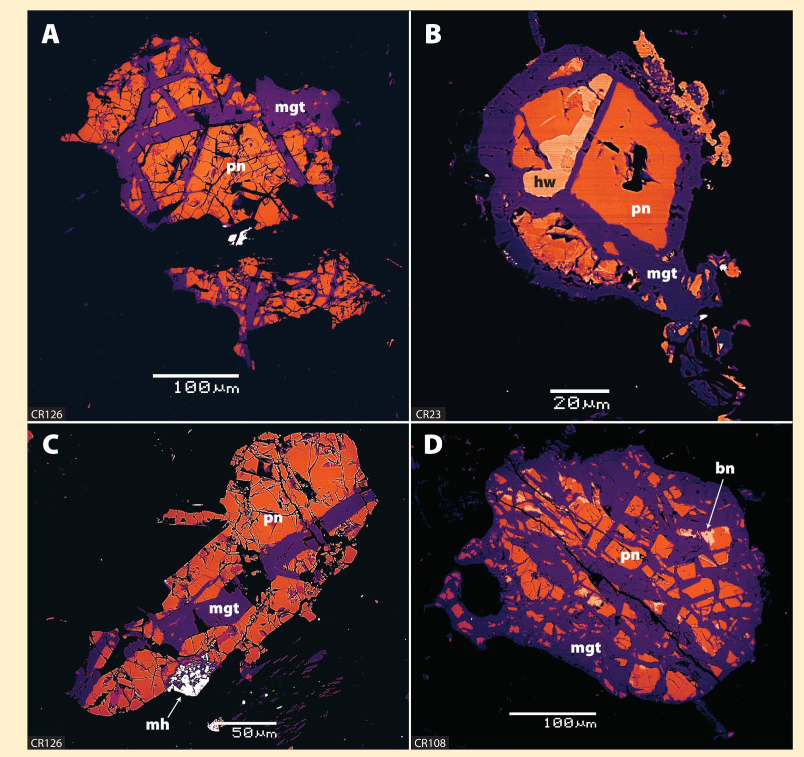

Figure 7. Pentlandite (pn) replaced **(A–D)** and enclosed **(B, D)** by magnetite (mgt). Heazlewoodite (hw) replacing pentlandite **(B)**. Bornite (bn) intergrown with pentlandite **(D)**. Maucherite (mh) intergrown with magnetite **(C)**.

Bismuthinite and parkerite(?)

Rare grains of Bi minerals are readily detected because of their high average atomic number, but too small for quantitative analysis. Some grains contain only Bi and S, and must be bismuthinite (Bi_2S_3). Others contain Bi, Ni, S, and variable Pb; these are probably parkerite, $Ni_3(Bi,Pb)_2S_2$.

Awaruite, Ni_5Fe

Perhaps the most exotic mineral we've found at CR is awaruite, an intermetallic compound of Ni and Fe (Howald, 2003). Awaruite is another mineral of serpentinites and, uncommonly, meteorites. In the western U.S., terrestrial (non-meteoritic) awaruite is previously reported from about three localities in the Coast Ranges of California and Oregon. At the Oregeon locality (same as orcélite), awaruite is also called josephinite (Dick, 1974).

At CR awaruite forms rare, minute ($\lesssim 5$ µm) blebs within magnetite, close to heazlewoodite (Fig. 9A). CR awaruite is Ni-rich, ≈ Ni_5Fe, near the middle of the range for awaruite coexisting with heazlewoodite determined by Sciortino et al. (2015) (Fig. 4).

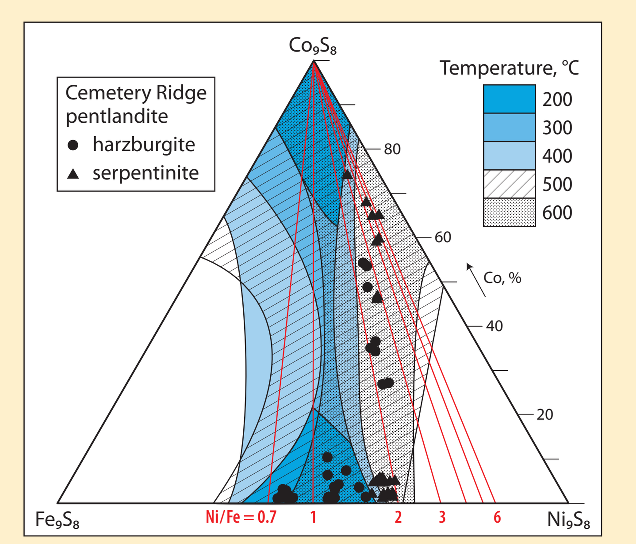

Figure 5. Composition of CR pentlandite; and stability fields for pentlandite (lower side), cobalt pentlandite (apex), and cobaltoan pentlandite (center) as a function of temperature (Kaneda et al., 1986). Note shift to greater Ni/Fe at higher T.

Table 2. The six Ni-arsenide minerals.[1]

Mineral	Formula	As/Ni
orcélite	$Ni_{4.75}As_2$	0.42
maucherite	$Ni_{11}As_8$	0.73
nickeline	NiAs	1.00
krutovite[2]	$NiAs_2$	2.00
rammelsbergite[2]	$NiAs_2$	2.00
pararammelsbergite[2]	$NiAs_2$	2.00

[1]Anthony et al., 1990; Bindi et al., 2014
[2]Trimorphs

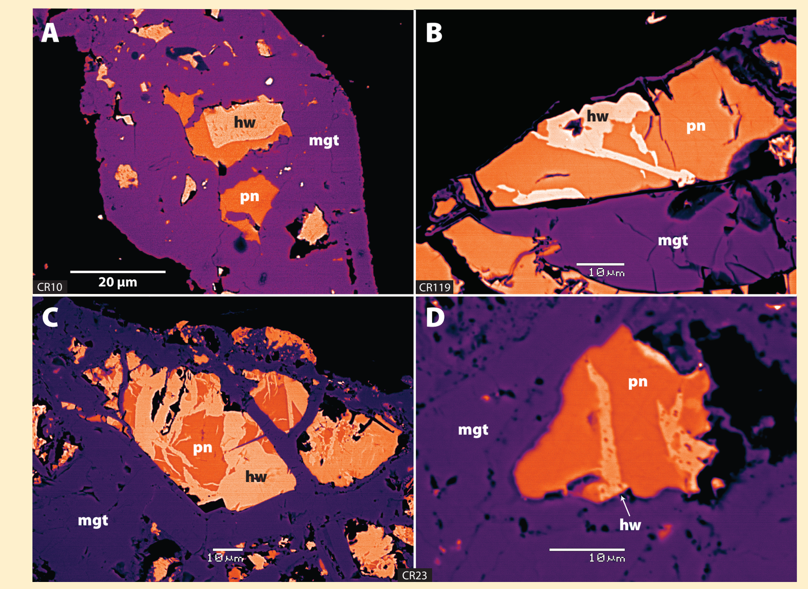

Figure 8. Apparently mutually stable pentlandite (pn) and heazlewoodite (hw) **(A)**. Pentlandite replaced **(B–D)** or enclosed **(C)** by heazlewoodite. Pentlandite and heazlewoodite replaced **(B, C)** or enclosed **(C, D)** by magnetite (mgt); also Fig. 7B.

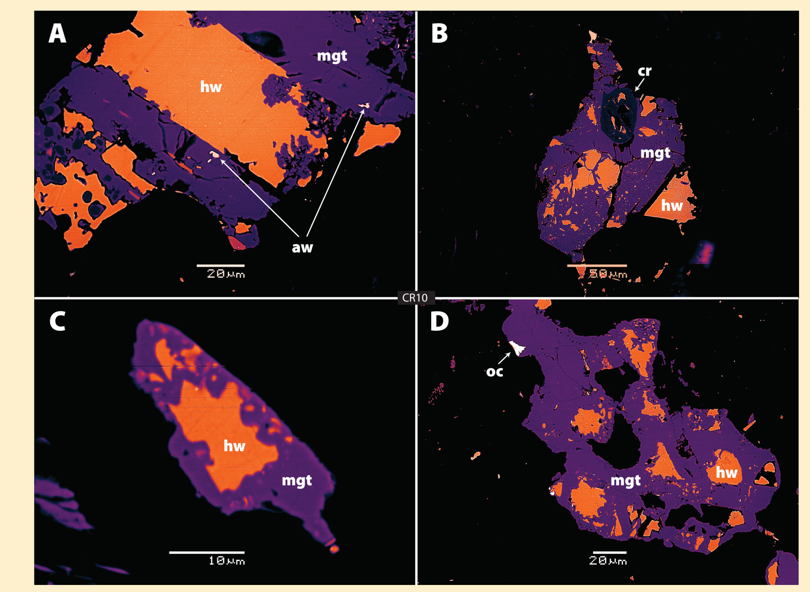

Figure 9. Heazlewoodite (hw) intergrown with and replaced by magnetite (mgt) **(A–D)** and enclosed by magnetite **(B, C, D)**; also Fig. 8C. Awaruite (aw) in magnetite near heazlewoodite **(A)**. Orcélite (oc) at the margin of magnetite **(D)**. Relict chromian spinel (cr) within magnetite **(B)**.

Paragenetic sequence

In least-serpentinized (Fig. 3A) CR harzburgite, pentlandite is partially replaced and in some places enveloped by magnetite (Fig. 7); heazlewoodite is absent. With increasing serpentinization, pentlandite and heazlewoodite form together (Fig. 8A), then pentlandite is replaced, and locally enveloped, by heazlewoodite (Fig. 8B–D). Concurrently, cobaltoan pentlandite becomes more common. In serpentinite, heazlewoodite is intergrown with and enveloped by magnetite (Fig. 9). Thus, the generalized paragenetic sequence (Fig. 10) is pentlandite → magnetite, pentlandite → heazlewoodite, heazlewoodite → magnetite. The latter two stages are preserved in some single grains within serpentinite (e.g., Figs. 7B; 8B–D). This paragenesis is consistent with decreasing sulfidation during progressive serpentinization (Figs. 3, 4).

Conditions of serpentinization

The subducted peridotite at Cemetery Ridge was serpentinized by seawater, probably in late Mesozoic western California (Haxel et al., 2015). Conditions of serpentinization are constrained by: widespread coexistence of pentlandite, heazlewoodite, and magnetite; absence of millerite, pyrite, and hematite; presence of traces of awaruite; and scarcity of troilite (pyrrhotite). This assemblage indicates a highly reduced pore fluid, typical of serpentinization of oceanic peridotite (Fig. 11). Specific positions of phase boundaries in Figure 11 are only approximately applicable to CR, as the temperature of serpentinization there probably exceeded 300 °C (Fig. 5). But, taking this phase diagram at face value, conditions during serpentinization of CR peridotite evidently were comparable to (though apparently slightly less reduced than) those in two well-documented oceanic areas. Despite its present unusual inland tectonic setting, CR serpentinite has much in common with other oceanic serpentinites.

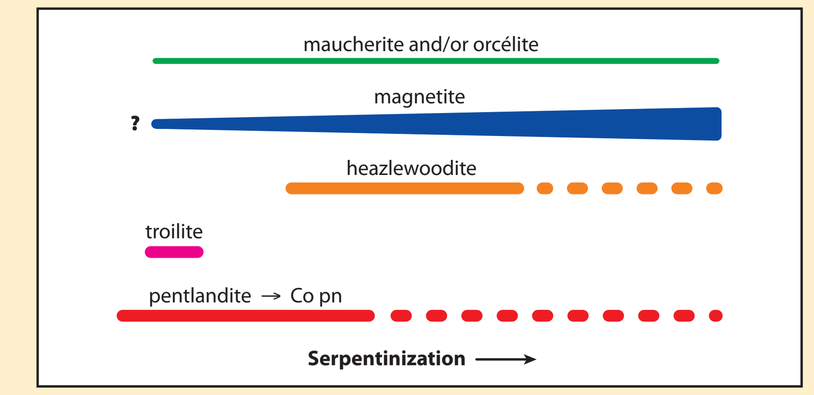

Figure 10. Generalized paragenetic sequence of serpentinite-hosted sulfides, magnetite, and arsenides at Cemetery Ridge. Solid lines indicate formation; dashed lines indicate persistence, possibly metastable.

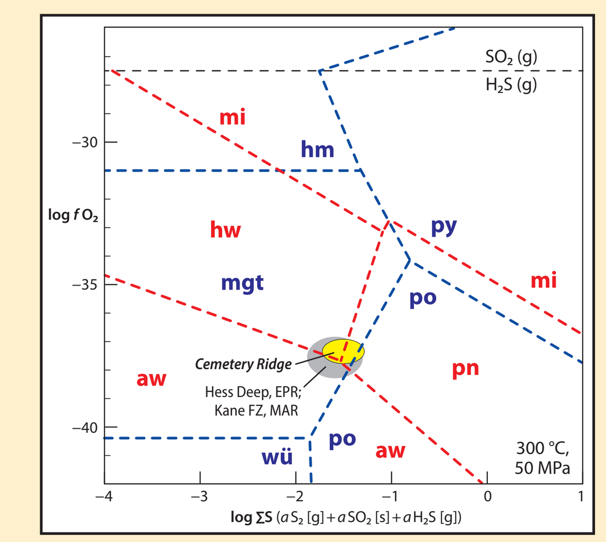

Figure 11. Phase stability in the Fe-S-O and Ni-S-O systems as a function of fO_2 and ΣS (after Foustoukos et al., 2015). Minerals (Fig. 4): aw, awaruite; hm, hematite; hw, heazlewoodite; mi, millerite; mgt, magnetite; pn, pentlandite; po, pyrrhotite; py, pyrite; wü, wüstite (FeO). EPR, East Pacific Rise; FZ, Fracture Zone; MAR, Mid-Atlantic Ridge.

New minerals for Arizona

Four minerals we've found at Cemetery Ridge are new for Arizona, where serpentinite is quite rare: heazlewoodite, awaruite, orcélite, and maucherite (cf. Anthony et al., 1995; on-line reports of awaruite in the Canyon Diablo meteorite are apocryphal). Terrestrial (non-meteoritic) troilite has not previously been reported from Arizona. Cobaltoan pentlandite (a mineral variety) very likely also is new to Arizona. As our study continues, we won't be surprised to find additional unusual minerals.

Funding

NSF Grant EAR-1347954 to Jacobson and Haxel; USGS, GMEG and Bradley; NAU; ISU.

Microprobe parameters

Cameca SX50, at NAU. Accelerating potential 20 kV, beam current 50 nA, spot size ≈ 1 µm, counting time 20 s per element. Standards: chalcopyrite, millerite, pyrite, Co metal, sphalerite, GaAs, InSb.

References Cited

Anthony, J.W., Bideaux, R.A., Blath, K.W., and Nichols, M.C., 1990, Handbook of mineralogy, vol. 1; Elements, sulfides, sulfosalts: Mineral Data Publishing, 588 p.

Anthony, J.W., Williams, S.A., Bideaux, R.A., and Grant, R.W., 1995, Mineralogy of Arizona (3rd ed.): Arizona, 508 p.

Bindi, L., Tredoux, M., Zaccarini, F., Miller, D.E., and Garuti, G., 2014, Non-stoichiometric nickel arsenides in nature: the structure of orcelite, $Ni_{5-x}As_2$ ($x = 0.25$), from the Bon Accord oxide body, South Africa: Journal of Alloys and Compounds, v. 601, p. 175–178.

Bowles, J.F.W., Howie, R.A., Vaughan, D.J., and Zussman, J., 2011, Rock-forming minerals, vol. 5; Non-silicates: oxides, hydroxides, and sulphides (2nd ed.): Geological Society of London, 920 p.

Dick, H.J.B., 1974, Terrestrial nickel-iron from the Josephine peridotite, its geologic occurrence, associations, and origin: Earth and Planetary Science Letters, v. 24, p. 291–298.

Foustoukos, D.I., Bizimis , M., Frisby, C., and Shirey, S.B., 2015, Redox controls on Ni-Fe-PGE mineralization and Re/Os fractionation during serpentinization of abyssal peridotite: Geochimica et Cosmochimica Acta, v. 150, p. 11–25.

Frost, B.R., 1985, On the stability of sulfides, oxides, and native metals in serpentinite: Journal of Petrology, v. 36, p. 21–63.

Gaines, R.V., Skinner, H.C., Foord, E.E., Mason, B., and Rosenzweig, A., 1997, Dana's new mineralogy (eighth edition): Wiley, 1819 p.

Harris, D.C., and Nickel, E.H., 1972, Pentlandite compositions and associations in some mineral deposits: Canadian Mineralogist, v. 11, p. 861–878.

Hattori, K., Takahashi, Y., Guillot, S., and Johanson, B., 2005, Occurrence of arsenic (V) in forearc mantle serpentinites based on X-ray absorption spectroscopy study: Geochimica et Cosmochimica Acta, v. 69, p. 5585–5596.

Haxel, G.B., Jacobson, C.E., Richard, S.M., Tosdal, R.M., and Grubensky, M.J., 2002, The Orocopia Schist in southwest Arizona: early Tertiary oceanic rocks trapped or transported far inland, *in* Barth, A., ed., Contributions to crustal evolution of the southwestern United States: Geological Society of America Special Paper 365, p. 99–128.

Haxel, G.B., Jacobson, C.E., and Wittke, J.H., 2015, Mantle peridotite in newly discovered far-inland subduction complex, southwest Arizona: initial report: International Geology Review, v. 57, p. 871–892.

Howald, R.A., 2003, The thermodynamics of tetrataenite and awaruite: A review of the Fe-Ni phase diagram: Metallurgical and Materials Transactions A, v. 34A, p. 1759–1769.

Jacobson, C.E., Dawson, M.R., and Postlethwaite, C.E., 1988, Structure, metamorphism, and tectonic significance of the Pelona, Orocopia, and Rand Schists, southern California, *in* Ernst, W.G., ed., Metamorphism and crustal evolution of the western United States (Rubey Volume VII): Prentice-Hall, p. 976–997.

Jacobson, C.E., Grove, M., Pedrick, J.N., Barth, A.P., Marsaglia, K.M., Gehrels, G.E., and Nourse, J.A., 2011, Late Cretaceous-early Cenozoic tectonic evolution of the southern California margin inferred from provenance of trench and forearc sediments: Geological Society of America Bulletin, v. 123, p. 485–506.

Kaneda, H., Takenouchi, S., and Shoji, T., 1986, Stability of pentlandite in the Fe-Ni-Co-S system: Mineralium Deposita, v. 21, p. 169–180.

Klein, F. and Bach, W., 2009, Fe-Ni-Co-O-S phase relations in peridotite-seawater interactions: Journal of Petrology, v. 50, p. 37–59.

Lorand, J.P. and Pinet, M., 1984, L'orcélite des péridotites de Beni Bousera (Maroc), Ronda (Espagne), Table Mountain et Blow-Me-Down Mountain (Terre-Neuve) et du Pinde Septentrional (Gréce): Canadian Mineralogist, v. 22, p. 553–560.

Porter, R., Zandt, G., and McQuarrie, N., 2011, Pervasive lower-crustal seismic anisotropy in southern California: Evidence for underplated schists and active tectonics: Lithosphere, v. 3, p. 201–220.

Sciortino, M., Mungall, J.E., and Muinonen, J., 2015, Generation of high-Ni sulfide and alloy phases during serpentinization of dunite in the Dumont sill, Quebec: Economic Geology, v. 110, p. 733–761.

False-color images with ImageJ
Process > Sharpen
Image > LUT > Gem
Image > Adjust > Color Balance > Red (as needed)
Rectangular selection, adjust; Image > Crop

April 2016; Flagstaff, AZ